







## Article

# Enhancement of Power Conversion Efficiency with Zinc Oxide as Photoanode and *Cyanococcus*, *Punica granatum* L., and *Vitis vinifera* as Natural Fruit Dyes for Dye-Sensitized Solar Cells

Ili Salwani Mohamad <sup>1,2</sup> , Mohd Natashah Norizan <sup>1,2,\*</sup> , Norsuria Mahmed <sup>2,3</sup>, Nurnaeimah Jamalullail <sup>1</sup>, Dewi Suriyani Che Halin <sup>2,3</sup> , Mohd Arif Anuar Mohd Salleh <sup>2,3</sup>, Andrei Victor Sandu <sup>4,\*</sup> , Madalina Simona Baltatu <sup>4,\*</sup>  and Petrica Vizureanu <sup>4,5</sup> 

<sup>1</sup> Faculty of Electronic Engineering & Technology, Universiti Malaysia Perlis (UniMAP), Arau 02600, Malaysia

<sup>2</sup> Centre of Excellence Geopolymer and Green Technology (CEGeoGTech), Universiti Malaysia Perlis (UniMAP), Arau 02600, Malaysia

<sup>3</sup> Faculty of Chemical Engineering & Technology, Universiti Malaysia Perlis (UniMAP), Arau 02600, Malaysia

<sup>4</sup> Department of Technologies and Equipments for Materials Processing, Faculty of Materials Science and Engineering, Gheorghe Asachi Technical University of Iasi, Blvd. Mangeron, No. 51, 700050 Iasi, Romania

<sup>5</sup> Technical Sciences Academy of Romania, Dacia Blvd 26, 030167 Bucharest, Romania

\* Correspondence: mohdnatashah@unimap.edu.my (M.N.N.); sav@tuiasi.ro (A.V.S.);

madalina-simona.baltatu@academic.tuiasi.ro (M.S.B.)



**Citation:** Mohamad, I.S.; Norizan, M.N.; Mahmed, N.; Jamalullail, N.; Halin, D.S.C.; Salleh, M.A.A.M.; Sandu, A.V.; Baltatu, M.S.; Vizureanu, P. Enhancement of Power Conversion Efficiency with Zinc Oxide as Photoanode and *Cyanococcus*, *Punica granatum* L., and *Vitis vinifera* as Natural Fruit Dyes for Dye-Sensitized Solar Cells. *Coatings* **2022**, *12*, 1781. <https://doi.org/10.3390/coatings12111781>

Academic Editor: Shang Wang

Received: 31 October 2022

Accepted: 18 November 2022

Published: 21 November 2022

**Publisher's Note:** MDPI stays neutral with regard to jurisdictional claims in published maps and institutional affiliations.



**Copyright:** © 2022 by the authors. Licensee MDPI, Basel, Switzerland. This article is an open access article distributed under the terms and conditions of the Creative Commons Attribution (CC BY) license (<https://creativecommons.org/licenses/by/4.0/>).

**Abstract:** Ruthenium N719 is a well-known material used as the dye in commercial dye-sensitized solar cell (DSSC) devices. However, it poses risks to human health and the environment over time. On the other hand, titanium dioxide (TiO<sub>2</sub>) has low electron mobility and high recombination losses when used as a photoanode in this photovoltaic technology device. In addition, using Ruthenium as the dye material harms the environment and human health. As an alternative sensitizer to compensate Ruthenium on two different photoanodes (TiO<sub>2</sub> and ZnO), we constructed DSSC devices in this study using three different natural dyes (blueberry, pomegranate, and black grape). In good agreement with the anthocyanin content in the fruits, black grape, with the highest anthocyanin content (450.3 mg/L) compared to other fruit dyes (blueberry—386.6 mg/L and pomegranate—450.3 mg/L), resulted in the highest energy conversion efficiency (3.63%) for the natural dye-based DSSC. Furthermore, this research proved that the electrical performance of natural dye sensitizer in DSSC applications with a ZnO photoanode is better than using hazardous Ru N719 dye with a TiO<sub>2</sub> photoanode owing to the advantage of high electron mobility in ZnO.

**Keywords:** dye-sensitized solar cells; natural dye; zinc oxide; titanium oxide; anthocyanin; renewable energy; solar cells

## 1. Introduction

The third generation of solar cell technology, known as the dye-sensitized solar cell (DSSC) or Gratzel Cell, uses the photovoltaic effect to turn solar energy (photons) into electricity [1]. Due to its low cost of production, straightforward fabrication method, and efficiency performance comparable to other photovoltaic technology devices, this cell has attracted much research since Gratzel and O'Regan first developed it in 1991 [2]. Resembling the photosynthesis process, in DSSC, a dye that serves as the absorber layer (such as chlorophyll) absorbs photons and excites the electrons in the valence band to the conduction band. The electrons are then transferred from the conduction band to the outer circuit via metal oxide material, and a redox process completes the circuit at the counter electrode [3].

DSSC is a sandwich cell, as shown in Figure 1, that consists of ITO-coated glass as the electrodes and mechanical support [4], a wide bandgap mesoporous oxide layer

photoanode [5] that serves to anchor the molecules of the dye sensitizer and acts as an electron transport medium, a dye which responsible for absorption of solar radiation for electron generation [6], and an electrolyte based on iodide/triiodide redox system between photosensitized photoanode and transparent conducting counter electrode [7]. Technically, the DSSC's working principle can be simplified into the following [5];

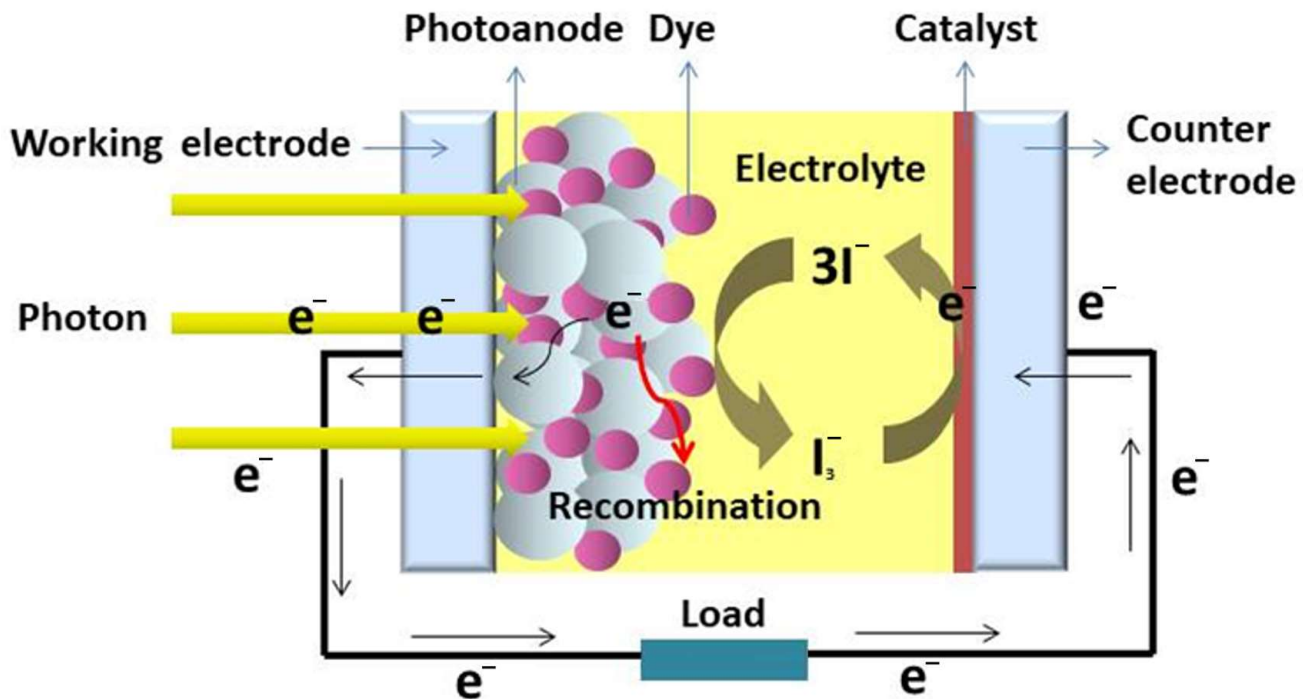


**Figure 1.** An electrical and chemical reaction in a DSSC structure during photon absorption.

A dye molecule ( $S$ ) is struck by photon energy ( $h\nu$ ), which causes it to enter the excited state ( $S^*$ ).



When an electron escapes from a dye molecule and enters a photoanode nanostructure, the molecule develops a hole ( $S^+$ ).



The redox system regenerates the dye molecule.



Electrons passing through the load regenerate the redox couple at the counter electrode.



The process will repeat in the presence of sunlight.

The commercialized DSSC utilizes  $TiO_2$  and metal complex N719, *Ruthenium* (Ru), as the photoanode and dye sensitizer. Due to their advantageous photoelectrochemical characteristics and great stability in the oxidized state, ruthenium complexes have attracted particular interest as photosensitizers in DSSC applications [8]. Modern DSSCs with ruthenium (II)- polypyridyl complexes (N719) as the active materials currently have total power conversion efficiencies of about 11% under AM1.5G light conditions [9]. Besides the extensive range of absorption from the visible to the near-infrared (NIR) spectrum, careful study of the HOMO and LUMO energy levels can be used to adjust the ruthenium

polypyridyl complexes' absorption spectra, which may increase the performance of the cell [10].

Unfortunately, besides the advantages listed above, the DSSC structure developed using  $\text{TiO}_2$  and Ru N719 have drawbacks that impact the device's performance and are carcinogenic.  $\text{TiO}_2$  has low electron mobility ( $0.1\text{--}4\text{ cm}^2\text{V}^{-1}\text{s}^{-1}$ ) [11], which causes the DSSC to have a high recombination rate [12]. This limitation of  $\text{TiO}_2$  reduces the number of carriers transported to the front contact and disturbs the overall cell efficiency performance. The red line in Figure 1 shows the electron recombination process phenomena, which results in a loss in energy conversion efficiency; it occurs when the electrons in the  $\text{TiO}_2$  structure recombine with the oxidized dye molecules and electrolyte rather than being transported to the anode and cathode terminals. In addition, because the  $\text{TiO}_2$  phase is metastable and can change into either brookite, anatase, or rutile under specific conditions such as temperature, the nanostructure of  $\text{TiO}_2$  is also restricted to being synthesized [13]. Ru, on the other hand, is a high-cost material [14], rare [15], and complex to be synthesized [16]. Worryingly, Ru sensitizer material has been reported as toxic and carcinogenic, harming human health [17]. It has been reported that the basic requirements for a good sensitizer are (a) a strong dye attached to a semiconductor material, (b) a broad absorption spectrum, and (c) being able to inject the electron into semiconductor materials [18].

In this work, we explored the possibility of using  $\text{ZnO}$ , which has higher electron mobility compared to  $\text{TiO}_2$ , as the photoanode for the test cells using three different organic dyes: *Cyanococcus* (Blueberry), *Punica granatum* L. (Pomegranate), and *Vitis vinifera* (Black Grape). Organic dyes were synthesized using chemical mixing, and the doctor blade technique was used to layer the photoanode material on the front contact of the respective devices. The properties of the photoanodes (morphology and phase) and the electrical performance of the DSSC devices with various photoanode materials and dyes used were reviewed, measured, and studied. Our previous study on natural pigments shows that photosensitizer dyes [19] such as chlorophyll, anthocyanin, and betalain extracted from various plants' leaves, flowers, and fruits have proved their efficacy as a good dye selection for organic-based DSSCs.

## 2. Materials and Methods

### 2.1. Preparation of $\text{TiO}_2$ and $\text{ZnO}$ Photoanode

Two transparent conductive oxide (TCO) coated glasses were cleaned as in [20]. Following this, 1 g of 99% anatase  $\text{TiO}_2$  powder and 1.5 mL of acetic acid solution (0.1 M) were combined in a pestle and mortar to create the  $\text{TiO}_2$  solution. A solution of 0.1 M acetic acid was prepared beforehand by mixing 10 mL of deionized water with 58  $\mu\text{L}$  of 99.99% acetic acid. A white soupy solution was then obtained by stirring the acetic acid solution and photoanode powder together. In the other pestle and mortar, 1 g of  $\text{ZnO}$  powder (98%) with 6 mL of ethanolic solution (0.01 M) and 0.5 mL of nitric acid solution (0.1 M) were mixed, creating a  $\text{ZnO}$  photoanode soupy solution. Ethanolic 0.01 M solutions were prepared beforehand by mixing absolute ethanol with DI water in a ratio of 7:3 to prevent photoanode paste from drying before applying it to the ITO-coated glass. Meanwhile, the 0.1 M nitric acid solution comprised 137  $\mu\text{L}$  of 65% nitric acid base and 20 mL of DI water.

$\text{TiO}_2$  and  $\text{ZnO}$  photoanodes were prepared using the doctor blade technique with a  $1.0 \times 1.5\text{ cm}^2$  active area on the conductive side of the ITO-coated glass, as shown in Figure 2. The deposited photoanode material was then annealed for 1 h at  $450\text{ }^\circ\text{C}$  in the ambient condition furnace.

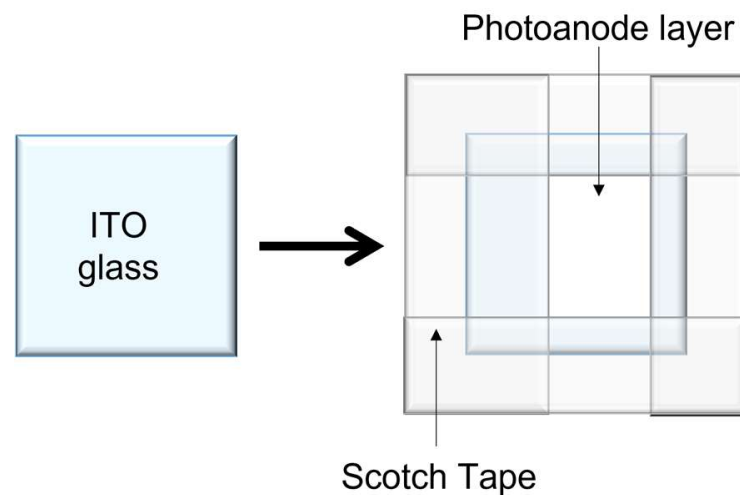


**Figure 2.** Photoanode semiconductor material deposition using the doctor blade method.

## 2.2. Preparation of Dye Sensitizers & Dye Coating Process

Due to the different environments and facilities of the laboratory where the DSSCs were fabricated, the efficiency of conventional DSSCs obtained in this study may differ from the literature. In order to determine the effect of photoanode and dye variations on the theoretical support hypothesis, a baseline cell of  $\text{TiO}_2$  with *Ruthenium* (Ru N719) dyes was constructed prior to the implementation of any improvements for comparison and justification. Ru N719 dye was prepared as [20] for the baseline sample. Natural dye extracts from blueberry, black grape, and pomegranate were then prepared by crushing 50 g of selected fruits using a mortar. The extracts were filtered and diluted in 20 mL of ethanol and the solutions in Figure 3 were obtained. According to previous research [21], the presence of ethanol in the dye solution can stabilize the acidity of the fruit dyes to prevent the photoanode from dissolving, which could reduce the DSSC's ability to convert sunlight into energy.

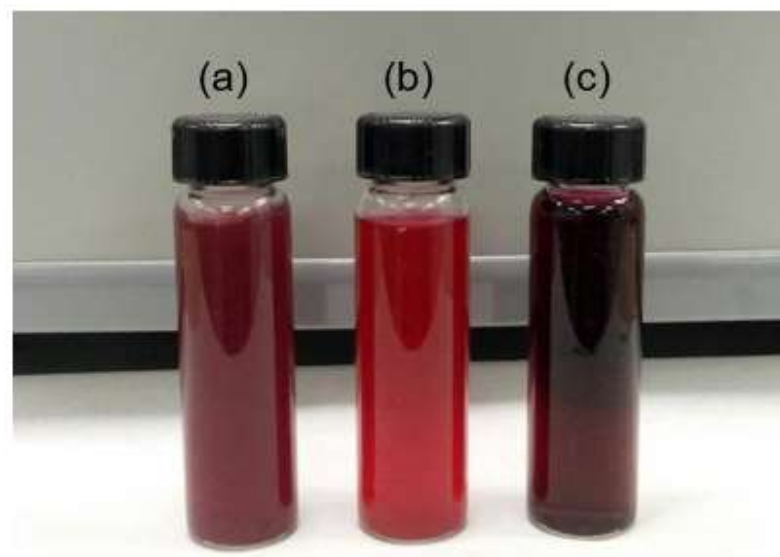


**Figure 3.** (a) black grape; (b) pomegranate, and (c) blueberry dye solutions.

As shown in Figure 4, the prepared photoanodes were immersed in the dye solution for two hours in a sealed petri dish.

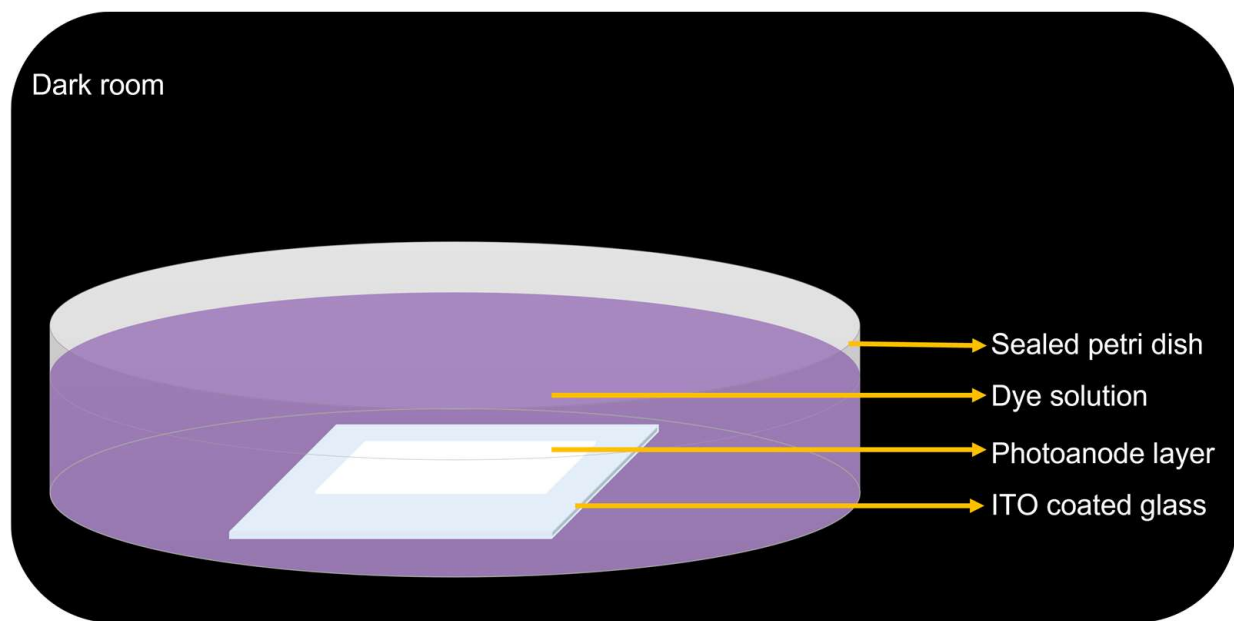


**Figure 4.** Photoanode dye coating process in dark ambient.

The longer time taken for this step may cause peel-off at the photoanode layer due to the acidity factor in the dyes. The samples were placed in a dark, enclosed area in a sealed petri dish covered in aluminum foil. Figure 5 shows the working electrode (photoanode) before and after the dye soaking process.

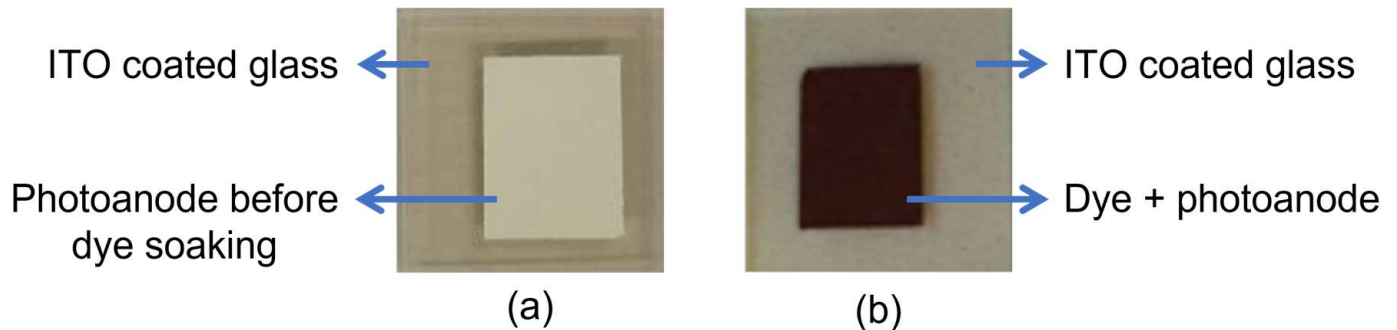


**Figure 5.** The working electrode (a) before the dye soaking process and (b) after 2 h of the dye coating process.

### 2.3. Preparation of Counter Electrode

On the ITO-coated glass, two holes with diameters of 1 mm and 0.5 mm were drilled. The 1-mm-size hole was created as the route for the electrolyte injection because the final DSSC will be sealed at the edge to prevent air from reducing the efficiency of the cell. The 0.5 mm hole served as a passageway for the trapped air in the DSSC structure to exit so that the electrolyte solution could fill the space between the two electrodes. Using the candle soot, the carbon layer with  $1.0 \times 1.5 \text{ cm}^2$  active area was deposited on the ITO-coated glass's conductive side. Finally, the excess carbon layer was rubbed using a cotton bud. Figure 6 shows the counter electrode's final product.

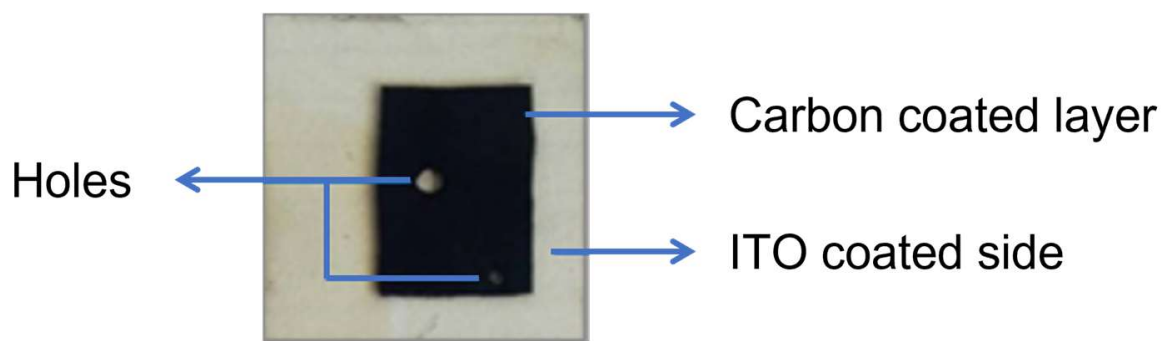


**Figure 6.** Carbon-coated counter electrode.

#### 2.4. Dye-Sensitized Solar Cells (DSSC) Assembly

DSSC was constructed by sandwiching a photoanode that was soaked in the dye with the counter electrode sealed with parafilm at the side (heated at 80 °C for 30 s with 500 g force applied on it to ensure that the DSSC was completely sealed). A potassium iodide (KI) solution that acts as an electrolyte was dropped into the sample through the hole at the counter electrode. The hole was then sealed by using scotch tape. The sample was then cooled at room temperature. This step is very important to prevent the electrolyte from leaking.

The electrical properties and energy conversion efficiency of the constructed DSSC were examined using a solar simulator (Keithley SMU 2450, Keithley, Tektronix, Beaverton, OR, USA). The DSSC was subjected to 1000 W/m<sup>2</sup> of light produced by a xenon lamp power supply (XPS-1600, Solar Light Inc., Glenside, PA, USA), simulating actual solar energy during the electrical testing. The current density–voltage (J–V) characteristics can be used to determine energy conversion efficiency. The efficiency of a solar cell is calculated from Equation (5) [22], where  $P_{in}$  is the input power from the sun at AM1.5G with a value of 1000 W/m<sup>2</sup>. This mathematical relation shows that  $J_{sc}$ ,  $V_{oc}$ , and  $FF$  are the three most important indicators that affect the output performance of a photovoltaic cell.

$$\eta = \frac{J_{sc} \times V_{oc} \times FF}{P_{in}} = \frac{J_{sc} \times V_{oc} \times FF}{I_{max} \times V_{max}} \quad (5)$$

where

$\eta$  = efficiency

$J_{sc}$  = short circuit current

$V_{oc}$  = open circuit voltage

$FF$  = fill factor

$P_{in}$  = input power

$I_{max}$  = maximum current

$V_{max}$  = maximum voltage

The factors affecting the energy conversion efficiency of the DSSC were examined through the crystallite size and structure of the photoanode, which were seen using an X-ray diffraction instrument (D2 Phaser, Bruker Ltd., Billerica, MA, USA). A scanning electron microscope (SEM, JOEL JSM-6010LV, JOEL Ltd., Tokyo, Japan) was also used to examine the surface morphology of each synthesized photoanode. ImageJ was used to determine the average particle size. The ability of the natural fruit dyes from blueberry, pomegranate, and black grape to absorb light was investigated using UV-visible spectroscopy (Lambda 950, Perkin Elmer, Inc., Waltham, MA, USA).

### 3. Results and Discussions

Based on the electrical performance testing for the laboratory baseline cell, the TiO<sub>2</sub>-based photoanode with inorganic Ru N719 dye recorded 1.31% compared to 2.22% for the ZnO-based photoanode DSSC with the same dye, as stated in Table 1. Compared to our



previous research in [20], 2 h of soaking time for the photoanode in the Ru N719 dye in this work has improved the electrical performance of both the TiO<sub>2</sub> and ZnO photoanode. TiO<sub>2</sub>-based photoanode DSSC portrayed better  $J_{sc}$  and a slightly higher fill factor than ZnO-based DSSC. However, in contrast, the ZnO photoanode shows a significant increment in  $V_{oc}$ , leading to better efficiency.

**Table 1.** Electrical performance for the TiO<sub>2</sub> and ZnO Baseline Cell with Ru N719 dye.

Dye	Photoanode	$J_{sc}$ (mA/cm <sup>2</sup> )	$V_{oc}$ (V)	Fill Factor (FF)	$\eta$ (%)
Ru N719	TiO <sub>2</sub>	7.47	0.36	0.59	1.31
	ZnO	5.18	0.79	0.54	2.22

The average crystallite size for TiO<sub>2</sub> and ZnO calculated using the Scherrer equation based on XRD evaluation were 18.76 nm and 19.30 nm, respectively. These findings validated that the ZnO photoanode measured energy conversion efficiency, which was 69.5% better than the TiO<sub>2</sub> photoanode containing Ru N719 dye.

The ZnO photoanode's magnificent improvement can be attributed to the morphological features in the photoanode layer, according to the results of the XRD analysis and SEM surface morphology identification in our earlier work. The ZnO photoanode layer's rectangular nanostructures, as seen in Figure 7, have a lot of surface area for the dye to adhere to, enabling the DSSC to absorb more energy [23].

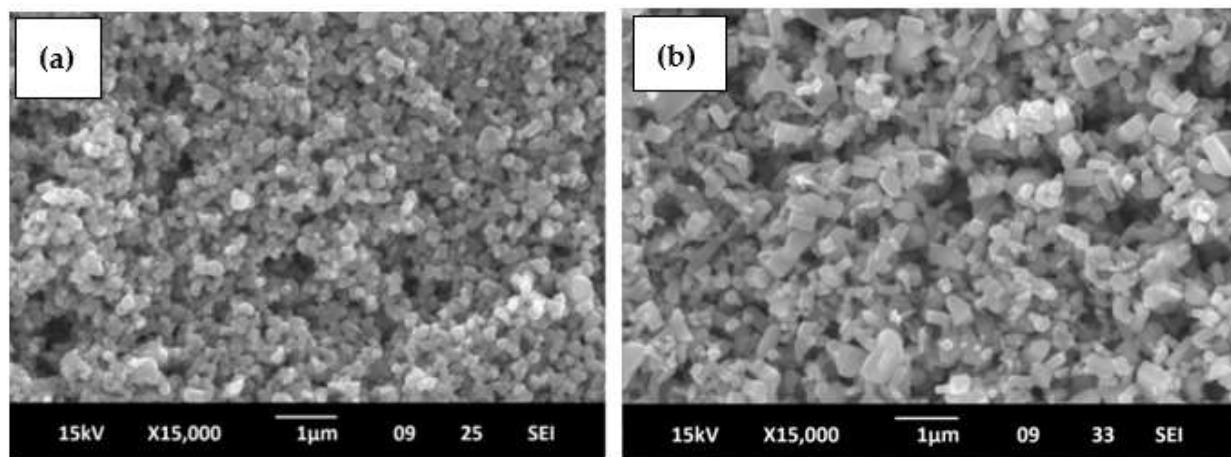


**Figure 7.** Surface morphology of SEM for (a) TiO<sub>2</sub> and (b) ZnO [20].

Furthermore, the larger ZnO photoanode structure, which consists of rectangular-shaped nanostructures, eventually creates a light-scattering layer and aids in enhancing the DSSC's capacity to harvest energy by reflecting light that passes through the photoanode layer so that the dye molecules can reabsorb it, as demonstrated by the analogy in Figure 8. This finding is well-concordant with earlier research [24].

The higher energy conversion efficiency of the ZnO photoanode is also supported by the material's chemical characteristics, which include high electron mobility (200 cm<sup>2</sup>V<sup>−1</sup>s<sup>−1</sup>) and large free excitation binding energy (60 meV) [25]. Thus, it was proved that ZnO has a higher energy conversion efficiency for a semiconductor photoanode than a TiO<sub>2</sub> photoanode.

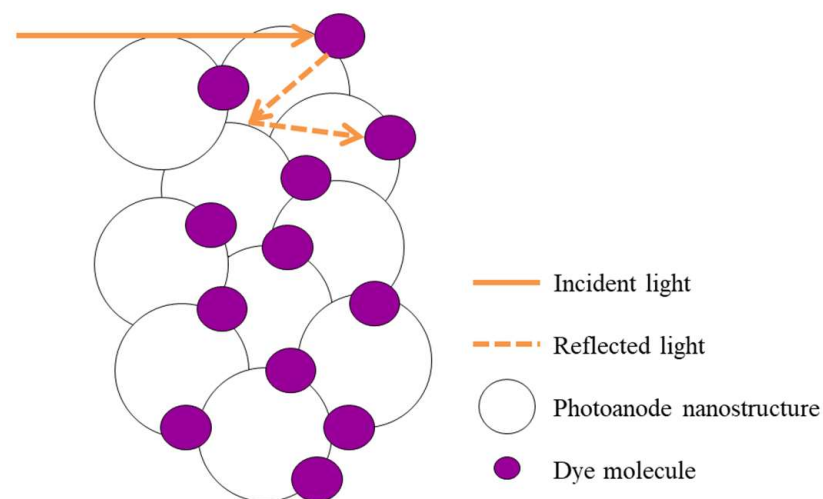


**Figure 8.** Light scattering effect on large particle size semiconductor photoanode material.

The electrical performance of DSSCs using various natural fruit dyes containing anthocyanin pigments is summarized in Table 2. The highest energy conversion efficiency for natural dye-based DSSC is found in the ZnO photoanode-based device with black grape dye (3.63%). We can observe that for all organic dyes, most ZnO-based DSSC was reported to give higher  $V_{oc}$  than TiO<sub>2</sub>-based DSSC. These findings are consistent with the hypothesis that materials with higher bandgap values have higher  $V_{oc}$  values, as in Equation (6) [26], which may be associated with slower recombination and better electron collection. This argument is backed by the characteristics of ZnO material, which is known to have better electron mobility than TiO<sub>2</sub> material, which further enhances electron transport and makes charge carrier separation easier. Different organic dyes used do not seem to affect  $V_{oc}$  significantly, but different photoanodes do.

$$qV_{OC} = \left(1 - \frac{T}{T_{sun}}\right) - kT \left[ \ln\left(\frac{\Omega_{emit}}{\Omega_{sun}}\right) + \ln\left(\frac{4n^2}{I}\right) - \ln(QE) \right] \quad (6)$$

**Table 2.** Electrical performance of the constructed DSSC using various photoanodes and dye types.

Dye	Photoanode	$J_{sc}$ (mA/cm <sup>2</sup> )	$V_{oc}$ (V)	FF	$\eta$ (%)
Blueberry	TiO <sub>2</sub>	0.82	1.18	0.40	0.39
	ZnO	7.12	0.79	0.50	2.81
Pomegranate	TiO <sub>2</sub>	5.86	0.35	0.45	0.93
	ZnO	7.12	0.71	0.60	3.03
Black grape	TiO <sub>2</sub>	6.69	0.52	0.30	1.05
	ZnO	9.72	0.73	0.51	3.63

In order to study the separation efficiency of photogenerated electrons and holes, a room temperature photoluminescence (PL) spectroscopy evaluation of the photoanodes (and dyes) is needed, which was not covered in this work. However, it is reported that the decrease in PL intensity indicates efficient electron-hole separation and long-lived carriers, which may effectively reduce the recombination of electrons and holes.

The highlight of this study is the utilization of ZnO-based photoanode soaked with different organic dye materials to see the effect and impact of the interaction between the anthocyanin level of the dyes (compared to the commercial Ru N719 dye) with ZnO semiconductor material photoanode to the performance of DSSC. The unique, organic dye materials selected were specifically from blueberry, pomegranate, and black grape, which—reflecting different anthocyanin levels (with different carboxylic group content)—produced a direct



proportional relationship between the anthocyanin content level and the electrical performance of the DSSC. With regards to our previous review on the natural pigment absorber material for photon absorption and efficient electrical conversion in [19], it can be seen that the results obtained from this study are better, as  $J_{sc} = 9.72 \text{ mA/cm}^2$ ,  $V_{oc} = 0.73 \text{ V}$ ,  $FF = 0.51$ , and efficiency = 3.63%. This result is not solely contributed by the absorber material used; the photoanode semiconductor material used as the electron transporter also significantly contributes to this result.

Figure 9 shows the trends in the short circuit current density-open circuit voltage ( $J_{sc}$ - $V_{oc}$ ) characteristics for each tested sample. Overall, it can be concluded that all ZnO-based photoanode cells are performing better than TiO<sub>2</sub>-based cells regardless of organic dyes tested with more convincing J-V curve shape patterns. These results support ZnO's role as a photoanode with higher electron mobility properties as a better solution for electron transport to the front contact of the device than TiO<sub>2</sub>. The shorter time for the electron to be transported to the electrode minimizes the recombination process, thus enhancing efficiency. Black grape recorded the highest efficiency with the best  $J_{sc}$  among all cells tested compared to the other natural dyes used. As the dye is important to function as the photon absorber and electron generator for the DSSC cell, black grape proves that a high anthocyanin content in a material is very important for the role. The advantage of using ZnO as a photoanode compared to TiO<sub>2</sub> in terms of output performance also has been proved in our previous research [20] utilizing Ru N719 dye as the sensitizer.

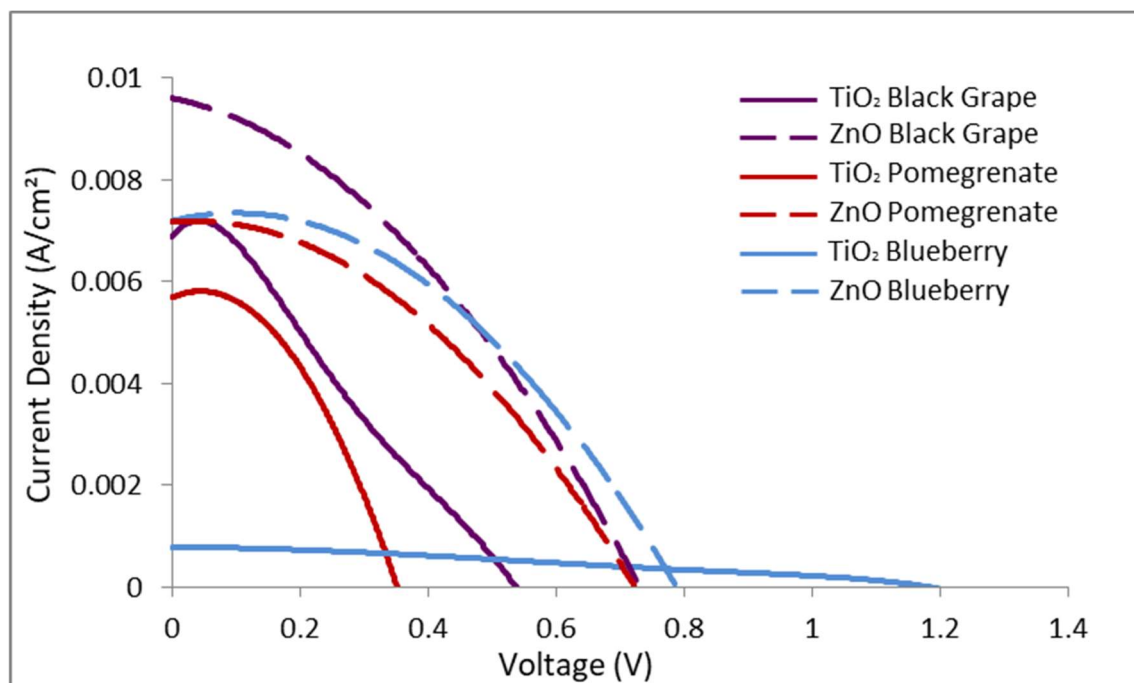


**Figure 9.** J-V curve for DSSCs with different types of photoanodes and dye sensitizers.

According to the trend in Figure 9, even though all DSSCs tested show a valid J-V curve for a practical photovoltaic (PV) device compared to the best DSSC cell reported by NREL, it has a lower fill factor, which can be seen at the area under the graph. The efficiency loss is partly due to the increased series resistance [27]. Series resistance can be caused by the unideal series connection of the electrodes, interfacial resistance between electrode and TCO, and electrolyte [28]. Series resistance also can be obtained from the following formula [29];

$$R_s = R_{TCO} + R_{CT} + R_{diff}(I_3^-) \quad (7)$$

where;

$R_{TCO}$  = substrate resistance

$R_{diff}(I_3^-)$  = diffusion impedance of  $I_3^-$  ions in the electrolyte

$R_{CT}$  = charge transfer resistance

Further work is needed to understand the detailed causes of loss due to series resistance to improve future device stability. A good solar cell must have near-zero series resistance and extremely high shunt resistance [30]. The absorption spectra of the dye extracts made from blueberry, black grape, and pomegranate are represented in Figure 10. The maximum absorption peaks (max) for blueberry, pomegranate, and black grape were seen at 568 nm, 539 nm, and 537 nm, respectively, corresponding to the anthocyanin pigments, which also matched the other study [31]. All anthocyanin dyes absorbed photons in UV (~350 nm) and visible light wavelengths.

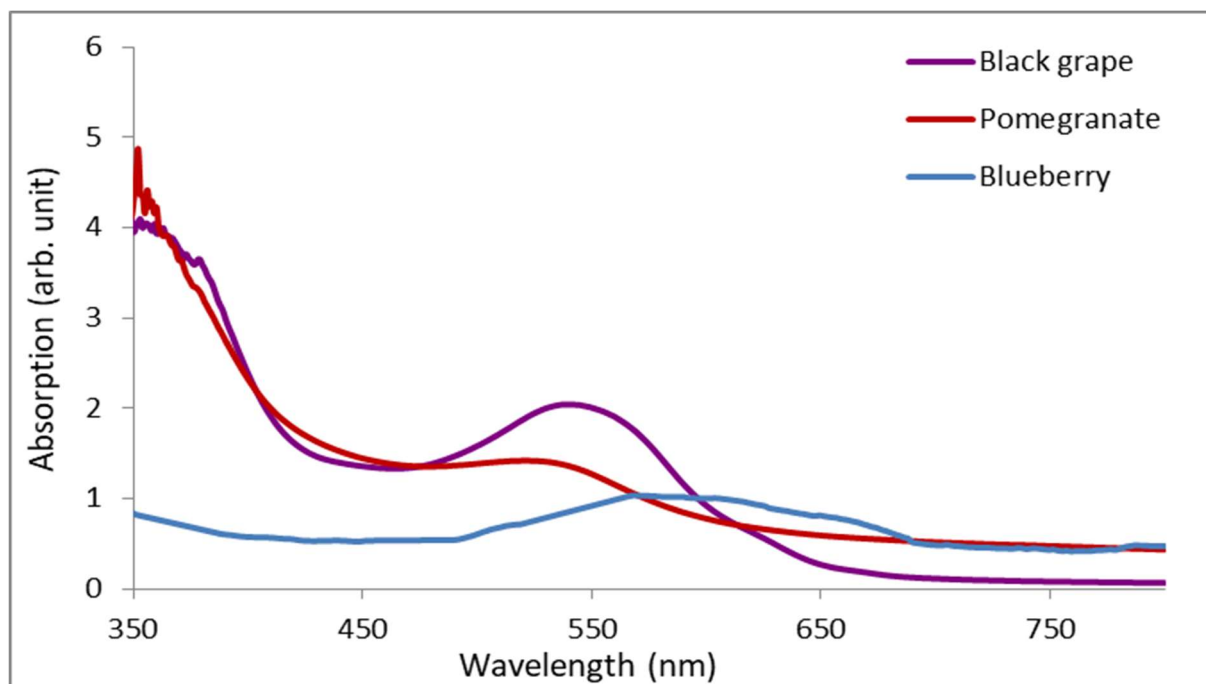


**Figure 10.** The absorption spectrum of anthocyanin fruit dyes.

The observed absorption peaks are congruent with the anthocyanin content. Black grape dye, having the highest anthocyanin content (450.3 mg/L) [32], shows high absorption and an intense peak compared to pomegranate (409.4 mg/L) [33] and blueberry dye (386.6 mg/L) [34]. Clearly, the trend of the  $\text{TiO}_2$  blueberry curve differs from that of the other curves in Figures 9 and 10. This is because the blueberry dye contains less anthocyanin than other organic dyes, which produces fewer electrons during the photon-to-electrical conversion when the cell is illuminated by sunlight. Therefore, based on the pattern curve, this cell has very high series resistance and very low shunt resistance. This research showed how fruit dyes contribute to a better DSSC's energy conversion efficiency due to anthocyanin contents in the dye. The anthocyanin dye pigments are attached to semiconductor photoanode structures thanks to the presence of carbonyl and hydroxyl ( $\text{COOH}$ ) group chains that serve as anchorage agents. The number of dye pigments attached to the semiconductor structure will determine how much sunlight can be absorbed by the DSSC.

The energy bandgap of the three anthocyanin fruit dyes was calculated by using equation  $E = hc/\lambda$ ; where  $h$  = Planck's constant ( $h = 6.63 \times 10^{-34}$ ),  $c$  = speed of light ( $c = 3 \times 10^8 \text{ ms}^{-1}$ ), and  $\lambda_{max}$  = wavelength of the maximum peak of UV-visible absorption spectrum [35]. Table 3 summarizes the energy bandgap of the anthocyanin fruit dyes:

blueberry (2.18 eV), pomegranate (2.30 eV), and black grape (2.32 eV). It can be observed that  $\lambda_{max}$  is inversely proportional to the energy bandgap of the anthocyanin dye. This is because a lower  $E_g$  material encounters a thermalization issue where the excess energy absorbed may turn into heat, leading to efficiency loss [36]. This justification supports our observation that the electrical performance of black grape dye with  $E_g$  2.32 eV gives an energy conversion efficiency of 3.63% higher than blueberry and pomegranate dye.

**Table 3.** Energy bandgap values of blueberry, pomegranate, and black grape dye.

Dye	$\lambda_{max}$ (nm)	The Energy Band Gap (eV)
Blueberry	568	2.18
Pomegranate	539	2.30
Black grape	537	2.32

#### 4. Conclusions

In this work, the performance of DSSC with organic and inorganic dyes has been examined in relation to the use of ZnO and TiO<sub>2</sub> as photoanodes. The ZnO photoanode has shown excellent performance due to having a bigger average crystallite and particle size in a rectangular shape compared to TiO<sub>2</sub> material, which helps to provide the light scattering layer and improves the light-harvesting ability of the DSSC. In addition, ZnO, with the advantage of high electron mobility (200 cm<sup>2</sup>V<sup>−1</sup>s<sup>−1</sup>) and large free excitation binding energy (60 meV), reduces the recombination loss in the cell. Based on three organic dyes selected for this research, black grapefruit (anthocyanin content 450.3 mg/L) obtained the highest efficiency compared to blueberry and pomegranate. Furthermore, this work proved that power conversion efficiency is directly proportional to the anthocyanin content level in dye material for organic dyes.

#### 5. Patents

The following code, PI2021004374, which corresponds to Malaysia, the country of origin of the invention, has been registered for patents resulting from the work described in this manuscript.

**Author Contributions:** Conceptualization, M.N.N. and I.S.M.; methodology, N.J., A.V.S. and I.S.M.; software, M.N.N.; validation, N.M., P.V. and D.S.C.H.; formal analysis, I.S.M., M.S.B. and N.M.; investigation, N.J., P.V., I.S.M. and M.N.N.; resources, N.M.; data curation, I.S.M. and A.V.S.; writing—original draft preparation, N.J.; writing—review and editing, I.S.M., M.S.B., M.N.N. and D.S.C.H.; visualization, M.N.N. and M.S.B.; supervision, I.S.M., M.N.N., A.V.S. and N.M.; project administration, I.S.M., M.N.N., P.V. and M.A.A.M.S.; funding acquisition, M.N.N. and M.A.A.M.S. All authors have read and agreed to the published version of the manuscript.

**Funding:** This research was funded by the Ministry of Higher Education of Malaysia (MoHE) and Universiti Malaysia Perlis (UniMAP) under the Fundamental Research Grant Scheme (FRGS) (Grant number: FRGS/1/2020/TK0/UNIMAP/02/35) and by Gheorghe Asachi Technical University of Iasi—TUIASI Romania, Scientific Research Funds, FCSU-2022.

**Institutional Review Board Statement:** Not applicable.

**Informed Consent Statement:** Not applicable.

**Data Availability Statement:** Not applicable.

**Acknowledgments:** Special thanks to the Centre of Excellence for Renewable Energy (CERE), and UniMAP for providing the characterization equipment.

**Conflicts of Interest:** The authors declare no conflict of interest.

#### References

1. O'Regan, B.; Grätzel, M. A Low-Cost, High-Efficiency Solar Cell Based on Dye-Sensitized Colloidal TiO<sub>2</sub> Films. *Nature* **1991**, *353*, 737–740. [[CrossRef](#)]

2. Pham, H.D.; Yang, T.C.; Jain, S.M.; Wilson, G.J.; Sonar, P. Development of Dopant-Free Organic Hole Transporting Materials for Perovskite Solar Cells. *Adv. Energy Mater.* **2020**, *10*, 1903326. [[CrossRef](#)]
3. Zaine, S.N.A.; Mohamed, N.M.; Khatani, M.; Samsudin, A.E.; Shahid, M.U. Trap State and Charge Recombination in Nanocrystalline Passivized Conductive and Photoelectrode Interface of Dye-Sensitized Solar Cell. *Coatings* **2020**, *10*, 284. [[CrossRef](#)]
4. Hossain, M.K.; Pervez, M.F.; Mia, M.N.H.; Mortuza, A.A.; Rahaman, M.S.; Karim, M.R.; Islam, J.M.M.; Ahmed, F.; Khan, M.A. Effect of Dye Extracting Solvents and Sensitization Time on Photovoltaic Performance of Natural Dye Sensitized Solar Cells. *Results Phys.* **2017**, *7*, 1516–1523. [[CrossRef](#)]
5. Devadiga, D.; Selvakumar, M.; Shetty, P.; Santosh, M.S. Recent Progress in Dye Sensitized Solar Cell Materials and Photo-Supercapacitors: A Review. *J. Power Sources* **2021**, *493*, 229698. [[CrossRef](#)]
6. Devadiga, D.; Selvakumar, M.; Shetty, P.; Santosh, M.S. Dye-Sensitized Solar Cell for Indoor Applications: A Mini-Review. *J. Electron. Mater.* **2021**, *50*, 3187–3206. [[CrossRef](#)]
7. Zeng, K.; Tong, Z.; Ma, L.; Zhu, W.-H.; Wu, W.; Xie, Y. Molecular Engineering Strategies for Fabricating Efficient Porphyrin-Based Dye-Sensitized Solar Cells. *Energy Environ. Sci.* **2020**, *13*, 1617–1657. [[CrossRef](#)]
8. Kohle, O.; Grätzel, M.; Meyer, A.F.; Meyer, T.B. The Photovoltaic Stability of Bis(Isothiocyanato)Ruthenium(II)-Bis-2, 2'-bipyridine-4, 4'-Dicarboxylic Acid and Related Sensitizers. *Adv. Mater.* **1997**, *9*, 904–906. [[CrossRef](#)]
9. Qin, Y.; Peng, Q. Ruthenium Sensitizers and Their Applications in Dye-Sensitized Solar Cells. *Int. J. Photoenergy* **2012**, *2012*, 291579. [[CrossRef](#)]
10. Tomar, N.; Agrawal, A.; Dhaka, V.S.; Surolia, P.K. Ruthenium Complexes Based Dye Sensitized Solar Cells: Fundamentals and Research Trends. *Sol. Energy* **2020**, *207*, 59–76. [[CrossRef](#)]
11. Chandiran, A.K.; Abdi-Jalebi, M.; Nazeeruddin, M.K.; Grätzel, M. Analysis of Electron Transfer Properties of ZnO and TiO<sub>2</sub> Photoanodes for Dye-Sensitized Solar Cells. *ACS Nano* **2014**, *8*, 2261–2268. [[CrossRef](#)] [[PubMed](#)]
12. Zhang, J.; Zhou, P.; Liu, J.; Yu, J. New Understanding of the Difference of Photocatalytic Activity among Anatase, Rutile and Brookite TiO<sub>2</sub>. *Phys. Chem. Chem. Phys.* **2014**, *16*, 20382–20386. [[CrossRef](#)] [[PubMed](#)]
13. Byrne, C.; Fagan, R.; Hinder, S.; McCormack, D.E.; Pillai, S.C. New Approach of Modifying the Anatase to Rutile Transition Temperature in TiO<sub>2</sub> Photocatalysts. *RSC Adv.* **2016**, *6*, 95232–95238. [[CrossRef](#)]
14. Alhamed, M.; Issa, A.; Doubal, A. Studying of Natural Dyes Properties as Photo-Sensitizer for Dye Sensitized Solar Cells (DSSC). *J. Electron Devices* **2012**, *16*, 1370–1383.
15. Hamadanian, M.; Safaei-Ghomi, J.; Hosseinpour, M.; Masoomi, R.; Jabbari, V. Uses of New Natural Dye Photosensitizers in Fabrication of High Potential Dye-Sensitized Solar Cells (DSSCs). *Mater. Sci. Semicond. Process.* **2014**, *27*, 733–739. [[CrossRef](#)]
16. Kushwaha, R.; Srivastava, P.; Bahadur, L. Natural Pigments from Plants Used as Sensitizers for TiO<sub>2</sub> Based Dye-Sensitized Solar Cells. *J. Energy* **2013**, *2013*, 654953. [[CrossRef](#)]
17. Calogero, G.; Bartolotta, A.; Di Marco, G.; Di Carlo, A.; Bonaccorso, F. Vegetable-Based Dye-Sensitized Solar Cells. *Chem. Soc. Rev.* **2015**, *44*, 3244–3294. [[CrossRef](#)]
18. Yahya, M.; Bouziani, A.; Ocak, C.; Seferoğlu, Z.; Sillanpää, M. Organic/Metal-Organic Photosensitizers for Dye-Sensitized Solar Cells (DSSC): Recent Developments, New Trends, and Future Perceptions. *Dye. Pigment.* **2021**, *192*, 109227. [[CrossRef](#)]
19. Jamalullail, N.; Mohamad, I.S.; Norizan, M.N.; Baharum, N.A.; Mahmed, N. Short Review: Natural Pigments Photosensitizer for Dye-Sensitized Solar Cell (DSSC). In Proceedings of the 2017 IEEE 15th Student Conference on Research and Development (SCoReD), IEEE, Putrajaya, Malaysia, 13–14 December 2018; Volume 2018, pp. 344–349.
20. Jamalullail, N.; Smohamad, I.; Nnorizan, M.; Mahmed, N. Enhancement of Energy Conversion Efficiency for Dye Sensitized Solar Cell Using Zinc Oxide Photoanode. *IOP Conf. Ser. Mater. Sci. Eng.* **2018**, *374*, 012048. [[CrossRef](#)]
21. Ayalew, W.A.; Ayele, D.W. Dye-Sensitized Solar Cells Using Natural Dye as Light-Harvesting Materials Extracted from Acanthus Sennii Chiovenda Flower and Euphorbia Cotinifolia Leaf. *J. Sci. Adv. Mater. Devices* **2016**, *1*, 488–494. [[CrossRef](#)]
22. Sánchez-García, M.A.; Bokhimi, X.; Maldonado-Álvarez, A.; Jiménez-González, A.E. Effect of Anatase Synthesis on the Performance of Dye-Sensitized Solar Cells. *Nanoscale Res. Lett.* **2015**, *10*, 306. [[CrossRef](#)] [[PubMed](#)]
23. Al-Agel, F.A.; Shaheer Akhtar, M.; Alshammari, H.; Alshammari, A.; Khan, S.A. Solution Processed ZnO Rectangular Prism as an Effective Photoanode Material for Dye Sensitized Solar Cells. *Mater. Lett.* **2015**, *147*, 119–122. [[CrossRef](#)]
24. Son, M.-K.; Seo, H.; Kim, S.-K.; Hong, N.-Y.; Kim, B.-M.; Park, S.; Prabakar, K.; Kim, H.-J. Analysis on the Light-Scattering Effect in Dye-Sensitized Solar Cell According to the TiO<sub>2</sub> Structural Differences. *Int. J. Photoenergy* **2012**, *2012*, 480929. [[CrossRef](#)]
25. Mohamad, I.S.; Ismail, S.S.; Norizan, M.N.; Murad, S.A.Z.; Abdullah, M.M.A. ZnO Photoanode Effect on the Efficiency Performance of Organic Based Dye Sensitized Solar Cell. *IOP Conf. Ser. Mater. Sci. Eng.* **2017**, *209*, 012028. [[CrossRef](#)]
26. Polman, A.; Atwater, H.A. Photonic Design Principles for Ultrahigh-Efficiency Photovoltaics. *Nat. Mater.* **2012**, *11*, 174–177. [[CrossRef](#)] [[PubMed](#)]
27. Zheng, J.; Mehrvarz, H.; Ma, F.-J.; Lau, C.F.J.; Green, M.A.; Huang, S.; Ho-Baillie, A.W.Y. 21.8% Efficient Monolithic Perovskite/Homo-Junction-Silicon Tandem Solar Cell on 16 Cm<sup>2</sup>. *ACS Energy Lett.* **2018**, *3*, 2299–2300. [[CrossRef](#)]
28. Koo, B.-K.; Lee, D.-Y.; Kim, H.-J.; Lee, W.-J.; Song, J.-S.; Kim, H.-J. Seasoning Effect of Dye-Sensitized Solar Cells with Different Counter Electrodes. *J. Electroceramics* **2006**, *17*, 79–82. [[CrossRef](#)]
29. Ramasamy, E.; Lee, W.J.; Lee, D.Y.; Song, J.S. Spray Coated Multi-Wall Carbon Nanotube Counter Electrode for Tri-Iodide (I<sub>3</sub><sup>-</sup>) Reduction in Dye-Sensitized Solar Cells. *Electrochem. Commun.* **2008**, *10*, 1087–1089. [[CrossRef](#)]

30. Amiri, O.; Salavati-Niasari, M. High Efficiency Dye-Sensitized Solar Cells (9.3%) by Using a New Compact Layer: Decrease Series Resistance and Increase Shunt Resistance. *Mater. Lett.* **2015**, *160*, 24–27. [\[CrossRef\]](#)
31. Ahliha, A.H.; Nurosyid, F.; Supriyanto, A.; Kusumaningsih, T. Optical Properties of Anthocyanin Dyes on TiO<sub>2</sub> as Photosensitizers for Application of Dye-Sensitized Solar Cell (DSSC). *IOP Conf. Ser. Mater. Sci. Eng.* **2018**, *333*, 012018. [\[CrossRef\]](#)
32. Hariram Nile, S.; Hwan Kim, D.; Keum, Y. Determination of Anthocyanin Content and Antioxidant Capacity of Different Grape Varieties. *Ciência e Técnica Vitivinícola* **2015**, *30*, 60–68. [\[CrossRef\]](#)
33. Alighourchi, H.R.; Barzegar, M.; Sahari, M.A.; Abbasi, S. Effect of Sonication on Anthocyanins, Total Phenolic Content, and Antioxidant Capacity of Pomegranate Juices. *Int. Food Res. J.* **2013**, *20*, 1703–1709.
34. TSUDA, T. Anthocyanins as Functional Food Factors— Chemistry, Nutrition and Health Promotion. *Food Sci. Technol. Res.* **2012**, *18*, 315–324. [\[CrossRef\]](#)
35. Dhafina, W.A.; Salleh, H.; Daud, M.Z.; Ghazali, M.S.M. Low Cost Dye-Sensitized Solar Cells Based on Zinc Oxide and Natural Anthocyanin Dye from Ardisia Elliptica Fruits. *Optik* **2018**, *172*, 28–34. [\[CrossRef\]](#)
36. Jasim, K.E. Quantum Dots Solar Cells. In *Solar Cells—New Approaches and Reviews*; InTech: London, UK, 2015.